

# Chapter 12

## Kinetic Modeling of Ammonia SCR for Cu-Zeolite Catalysts

Louise Olsson

In this chapter, kinetic models for ammonia SCR over Cu-zeolites are described. Both global and detailed models are presented and both commercial materials as well as model samples are used. In the SCR system, several reactions are important in order to describe the mechanism and these reactions are discussed below. Ammonia storage and desorption on the catalyst surface is crucial in order to capture the transient behavior of the catalytic system. These steps are examined using both temperature programmed desorption experiments, as well as with the help of microcalorimetry techniques. In more detailed kinetic models, adsorption of other species like water and  $\text{NO}_x$  are also considered. Depending on the  $\text{NO}_2$  to  $\text{NO}_x$  ratio, different SCR reactions will occur; standard SCR, rapid SCR, and slow  $\text{NO}_2$  SCR. These reactions are added to kinetic models, either in global format or more detailed reaction steps. In addition, there are several other reactions occurring during the SCR process, such as, for example, NO oxidation to produce  $\text{NO}_2$ . Unfortunately, there are also several unwanted side reactions taking place, like ammonia oxidation and  $\text{N}_2\text{O}$  formation. These steps are crucial to add to kinetic models and are described in this chapter.

### 12.1 Introduction

An important group of catalysts for  $\text{NO}_x$  reduction through ammonia SCR is represented by copper exchanged zeolites [1–9]. Many different zeolites have been investigated, for example, Cu-ZSM-5 [10–13], Cu-faujasite [14], Cu-Beta [15, 16], and Cu-Y [17]. Recently, copper zeolites with chabazite (CHA) structure have received great attention due to their high thermal stability and hydro carbon resistance [18]. Both Cu-SAPO-34 [19] and Cu-SSZ-13 [18] have a CHA structure

---

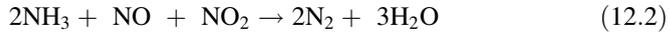
L. Olsson (✉)

Competence Centre for Catalysis, Chemical Engineering, Chalmers University  
of Technology, SE-412 96 Gothenburg, Sweden  
e-mail: louise.olsson@chalmers.se

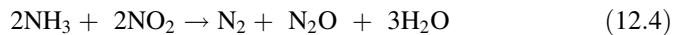
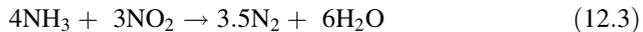
and have been investigated for  $\text{NH}_3$  SCR. The  $\text{NO}_x$  conversion depends on the  $\text{NO}_2$  ratio in the feed. When only NO is present, the standard SCR reaction occurs as follows:



while if equimolar amounts of NO and  $\text{NO}_2$  are present, the fast SCR reaction dominates at a much higher rate:



However, if the  $\text{NO}_2$  to  $\text{NO}_x$  ratio is high, the slow  $\text{NO}_2$  SCR reaction occurs while the amount of  $\text{N}_2\text{O}$  produced is also increased:



Kinetic models for ammonia SCR have been developed for vanadia on titania [20–24], Cu-ZSM-5 [10–13], Cu-faujasite [14], HZSM-5 [25], and Fe zeolites [26–28]. In this chapter, the focus is on kinetic models for ammonia SCR over copper zeolites. Both global and detailed kinetic models will be described and many subreactions in the mechanism, such as ammonia storage, ammonia oxidation, NO oxidation etc., will be discussed in detail.

## 12.2 Kinetic Models for Ammonia and Water Storage Over Cu-Zeolites

The copper zeolites store large amounts of ammonia. This is an important feature of these catalysts, since ammonia stored at the surface at medium temperatures can be used at low temperatures, where it is not possible to dose urea due to by-product formation. It is, therefore, crucial to describe ammonia storage and desorption in a kinetic model accurately to be able to predict transient variations.

The most common way to describe ammonia adsorption and desorption in SCR catalysts, in general, is to use the Temkin type isotherm [10, 13, 24, 27, 29]. The Temkin adsorption isotherm considers the adsorbate-adsorbate interactions, and in the models therefore coverage dependent heat of adsorption is used. This also results in that the activation energy for desorption of  $\text{NH}_3$  is coverage dependent:

$$E_{\text{des}} = E_{\text{des}}(0)(1 - \alpha\theta_{\text{NH}_3}) \quad (12.5)$$

where  $E_{\text{des}}(0)$  is the activation energy for desorption for zero coverage,  $\alpha$  is a constant, and  $\theta_{\text{NH}_3}$  is the coverage of ammonia on the surface. The heat of adsorption can be determined by fitting parameters to TPD experiments, which is the most common method. However, calorimetry is a powerful technique for measuring the heat of adsorption directly [16]. The advantage of this method is

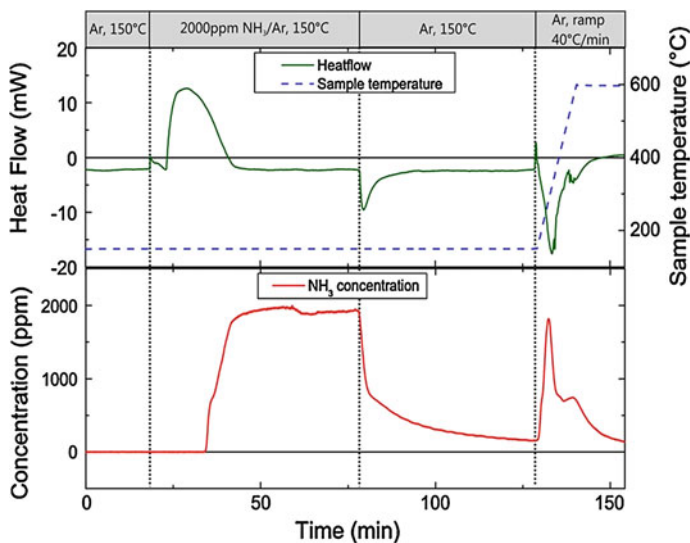


**Fig. 12.1** Ammonia TPD experiment on Cu-Beta. The top panel shows the heat flow and the lower panel the ammonia concentration [16]. Reprinted with permission from Wilken et al. [16]. Copyright (2010) Elsevier

that it measures  $\Delta H$ , thereby avoiding correlations between some of the parameters (for example, between the pre-exponential factor and activation barrier for desorption). Heat of adsorption of ammonia on zeolites has been measured previously, resulting in  $\Delta H$  for zero coverage of  $-130$  kJ/mol for H-ZSM-5 ( $\text{SiO}_2/\text{Al}_2\text{O}_3$  ratio of 30) [30],  $-130$  kJ/mol for H-Beta ( $\text{SiO}_2/\text{Al}_2\text{O}_3$  ratio of 19.6) [30] and  $-120$ – $130$  kJ/mol for H-ZSM-5 ( $\text{SiO}_2/\text{Al}_2\text{O}_3$  ratio of 110) [31]. Average  $\Delta H$  is also reported, resulting in  $-114$  kJ/mol for H-ZSM-5 ( $\text{SiO}_2/\text{Al}_2\text{O}_3$  ratio of 110) [31] and  $-104.8$  kJ/mol for Cu-ZSM-5 ( $\text{SiO}_2/\text{Al}_2\text{O}_3$  ratio of 30) [32].

Wilken et al. [16] conducted an ammonia TPD experiment in the calorimeter, while simultaneously measuring the heat produced/used, the results of which are shown in Fig. 12.1. In this experiment, the Cu-BEA catalyst is exposed to 2,000 ppm  $\text{NH}_3$ , which results in an exotherm and simultaneously there is a total uptake of all ammonia. When the catalyst is saturated with ammonia, ammonia breaks through and no heat is released. After the ammonia step, the catalyst is flushed with Ar only and weakly bound ammonia is released. This reaction is endotherm and heat is consumed (see top panel Fig. 12.1). In the last step, the temperature is increased and ammonia is desorbing. This experiment resulted in an average heat of adsorption of about  $-100$  kJ/mol [16]. However, as mentioned above, the heat of adsorption of ammonia is coverage dependent. Wilken et al. [16] developed a method for determining the coverage dependent heat of adsorption at atmospheric pressure. Initially, the catalyst was exposed to ammonia at  $500$  °C (see Fig. 12.2). Only the most strongly bound ammonia is adsorbed at this high temperature, which results in a low ammonia coverage with high  $\Delta H$ . The catalyst

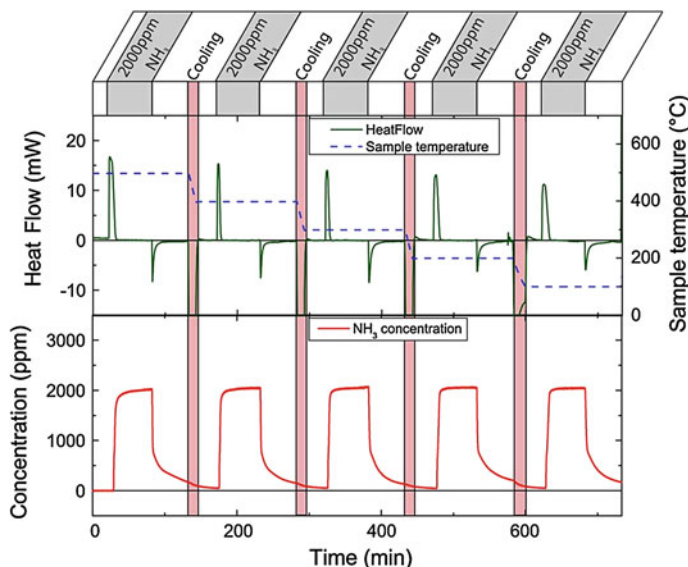
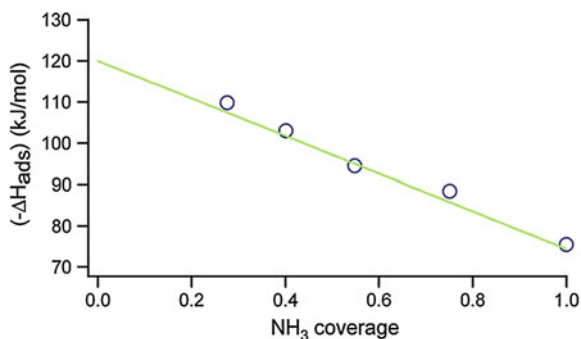


**Fig. 12.2** Stepwise ammonia adsorption experiment over Cu-Beta [16]. Reprinted with permission from Wilken et al. [16]. Copyright (2010) Elsevier

**Fig. 12.3** Heat of adsorption versus ammonia coverage, where the circles represent experimental values and the line is a linear fit [16]. Reprinted with permission from Wilken et al. [16]. Copyright (2010) Elsevier



is, thereafter, exposed to Ar only and the temperature decreases to 400 °C. At this temperature, another ammonia step is performed which results in a lower heat of adsorption. This procedure is repeated at 300, 200, and 100 °C (see Fig. 12.2), which results in lowering the heat released for each step. The results of this stepwise ammonia adsorption experiment are used to calculate the heat of adsorption and the corresponding ammonia coverage on the surface, which is described in more detail in Ref. [16]. These results are shown in Fig. 12.3.

The results clearly show a linear dependence of the heat of adsorption as a function of ammonia coverage. A linear fit of the experimental points results in:

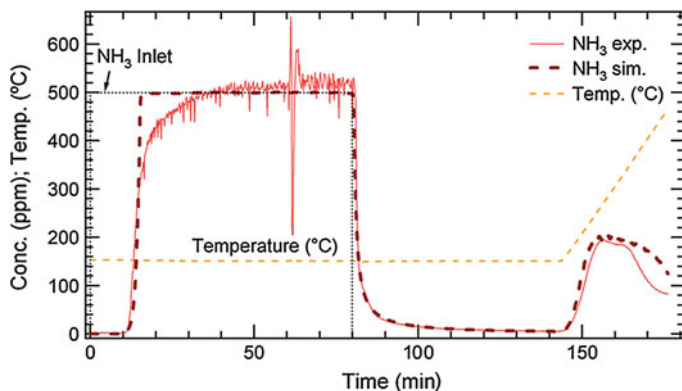


**Fig. 12.4** Experiment (*solid line*) and simulation (*dashed line*) from an  $\text{NH}_3$  TPD experiment over Cu-ZSM-5 catalyst [10]. Reprinted with permission from Olsson et al. [10]. Copyright (2008) Elsevier

$$E_{\text{desorption, NH}_3} = 120.0 \cdot (1 - 0.38 \cdot \theta_{\text{NH}_3}) \quad (12.6)$$

The microcalorimetry data have been successfully used in kinetic models (not shown here).

### 12.2.1 Global Kinetic Model for Ammonia Storage and Desorption

In an earlier study, Olsson et al. [10] fitted the parameters for ammonia adsorption and desorption to an ammonia TPD experiment conducted over Cu-ZSM-5, using coverage dependent activation energy for ammonia desorption, occurring on one storage site S1 according to:



The results of the experiment and model are shown in Fig. 12.4. Initially, there is a total uptake of all ammonia for about 10 min. This is followed by a breakthrough of ammonia until saturation is reached. After about 80 min, the ammonia is shut off and some weakly bound ammonia is released. Finally, the temperature is increased and a large ammonia desorption follows. The desorption peak is broad and contains a shoulder. Thus, there are different types of ammonia storage sites available in the catalyst. The model (see Fig. 12.4) describes this broad feature well by a coverage dependent heat of adsorption. It should be mentioned that S1, which is used in the global kinetic model is the total amount of sites that can adsorb ammonia, thus likely covering both Brønsted acid sites as well as different copper sites.

### 12.2.2 Detailed Kinetic Model for Ammonia and Water Storage

In addition, detailed kinetic models for ammonia adsorption and desorption [13], NO oxidation [11], and SCR [12] over Cu-ZSM-5 was developed. The active sites for all reactions are, in this model, the copper sites, which are denoted S1a and the amount determined from ICP-AES. In addition, on this site, all the molecules can adsorb ( $\text{NH}_3$ ,  $\text{O}_2$ ,  $\text{NO}_2$ ,  $\text{H}_2\text{O}$ ). However, according to electron paramagnetic resonance studies (EPR) [33, 34] and density functional theory calculations [17], it has been previously suggested in the literature that copper is capable of coordinating up to four ammonia molecules. This is in accordance with the mechanism for SCR by Komatsu et al. [35], where four ammonia molecules are attached to copper. We, therefore, used up to four ammonia molecules, bound to each copper site [13] and practically this is done by introducing S1b, where ammonia can adsorb. S1b is three times larger than the amount of copper sites, resulting in that S1a + S1b is four times larger than the Cu-sites. Further, water was also found to adsorb in large quantities and therefore, water is adsorbed on S1b. In the surface description also, acid sites, denoted S2, and physisorbed sites, denoted S3 are included. In this section, the ammonia storage and desorption is described and in the following sections details are given for the other adsorbates as well as the reactions. The results of the detailed ammonia storage kinetic model together with an ammonia TPD experiment conducted at room temperature, are shown in Fig. 12.5a and the calculated mean coverages in Fig. 12.5b. The calculated coverages suggest that ammonia on the Brønsted acid sites (S2) and ammonia on S1b (copper site, where ammonia and water adsorb) is the most strongly bound ammonia. The strength of ammonia on the copper site responsible for the reactions (S1a), was critical in order not to block the adsorption of oxygen and  $\text{NO}_x$  species, and thereby the activity for the different reactions. Both the global (see Fig. 12.4) and detailed (see Fig. 12.5) kinetic models describe the experimental features well, except for the slow storage of ammonia when the catalyst is close to saturation. It is possible that there is a mass-transport limitation or sterical hindrance when reaching saturation that causes this behavior. However, when examining the total amount of ammonia stored, this discrepancy is only a small fraction. In addition, in a real application, the catalyst will never be completely saturated since a very large ammonia slip would then occur.

Further, a detailed model of water adsorption and desorption was developed; the results of a water TPD experiment are shown in Fig. 12.6 [13]. Water is released with a distinct peak at lower temperature; however, water continues to be released up to very high temperatures. These results clearly demonstrate the complex interactions between water and zeolite.

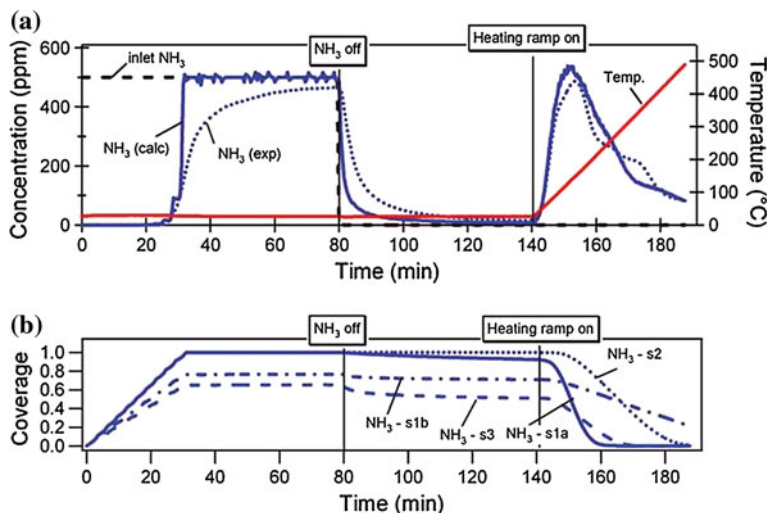
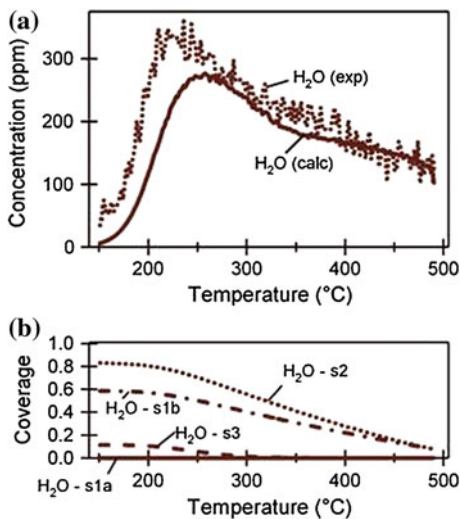


**Fig. 12.5** Ammonia TPD experiment at room temperature over Cu-ZSM-5. **a** The concentrations of ammonia from the experiment and model. **b** The calculated mean coverages [13]. Reprinted with permission from Sjövall et al. [13]. Copyright (2009) American Chemical Society

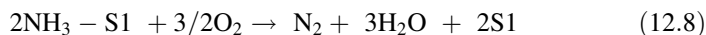
**Fig. 12.6** Water TPD experiment over Cu-ZSM-5. **a** The concentrations of water from the experiment and model. **b** The calculated mean coverages [13]. Reprinted with permission from Sjövall et al. [13]. Copyright (2009) American Chemical Society



## 12.3 Kinetic Models for Ammonia Oxidation Over Cu-Zeolites

### 12.3.1 Global Kinetic Model for Ammonia Oxidation

At high temperature, ammonia is oxidized by oxygen, which decreases the selectivity of the standard SCR reaction. In a kinetic model that should describe a broad temperature interval, it is therefore crucial to have a good description of the ammonia oxidation. Accordingly, we investigated ammonia oxidation separately in order to decrease the correlation between the parameters. In the global kinetic model, the following reaction was added in which ammonia stored on the surface is oxidized to produce  $N_2$  and  $H_2O$ :



Since no by-products like NO or  $N_2O$  were observed during ammonia oxidation, these reactions were excluded from the model. The results from the model and experiment are shown in Fig. 12.7 [10]. Prior to this experiment, the catalyst was pretreated with oxygen at high temperature in order to clean the surface from ammonia. When introducing the gas mixture consisting of ammonia, oxygen, and water, there was a long total uptake of ammonia attributable to the large storage [10]. At low temperature, no ammonia oxidation is observed and ammonia desorption is only visible when the temperature increases. However, significant ammonia oxidation is observed from 300 °C and increases with increasing temperature.

### 12.3.2 Detailed Kinetic Model for Ammonia Oxidation

Ammonia oxidation was included in the detailed model [12] (results not included). In this model, two reaction steps were added, where ammonia on the surface was oxidized either with oxygen alone or in a second step in a combination with hydroxyl groups. The hydroxyls are produced according to:



It was essential to add the reaction step, where ammonia reacts with hydroxyl groups in the detailed model, since the coverage of hydroxyl groups was large on the surface, but the simultaneous ammonia conversion only slightly decreased. Without this reaction step, the ammonia oxidation rate was significantly too low in the presence of water. For the global model described in Ref. [10], the effect of water was not included since all experiments contained high levels of water, and the model was therefore tuned in the presence of water.

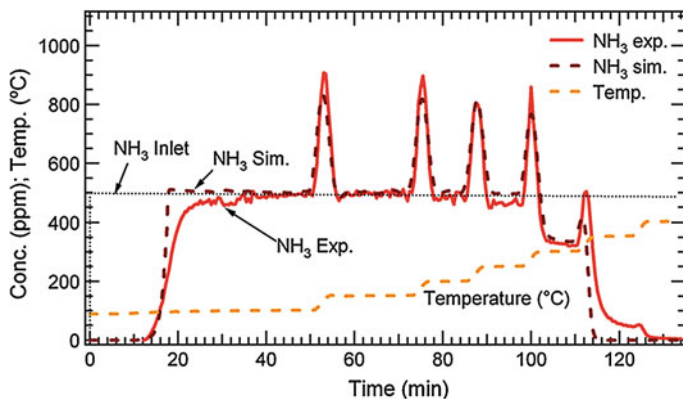


**Fig. 12.7** Ammonia oxidation over Cu-ZSM-5 using 8 % O<sub>2</sub>, 5 % H<sub>2</sub>O, and 500 ppm NH<sub>3</sub> [10]. Reprinted with permission from Olsson et al. [10]. Copyright (2008) Elsevier

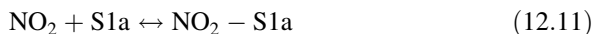
## 12.4 Kinetic Models for NO<sub>x</sub> Storage and NO Oxidation Over Cu-Zeolites

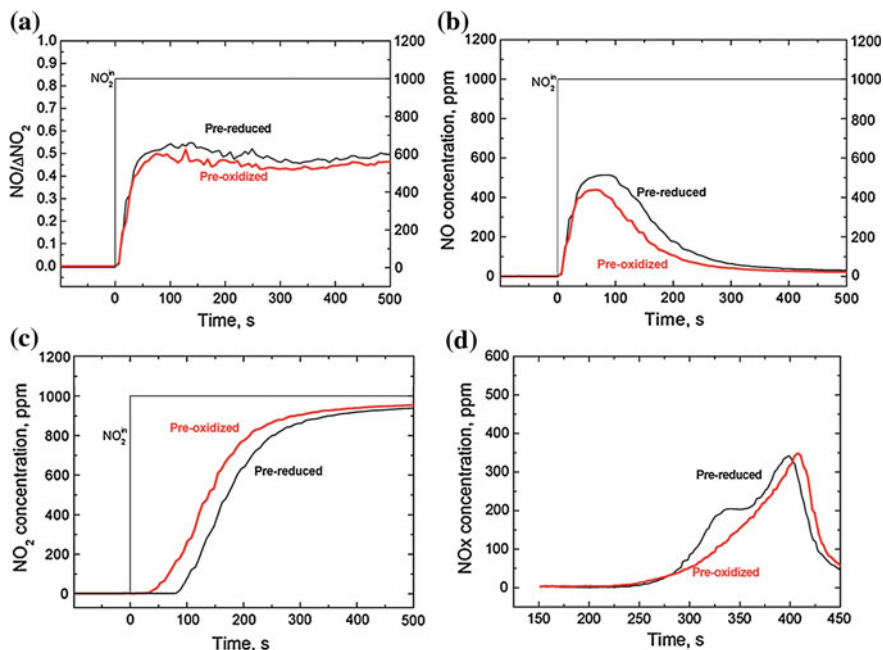
### 12.4.1 Detailed Kinetic Model for NO Oxidation

NO<sub>x</sub> storage is observed over copper zeolites [11, 36]. Colombo et al. [36] examined the NO<sub>2</sub> storage over pre-oxidized and pre-reduced Cu-CHA, with the results shown in Fig. 12.8. Slightly more NO is observed during the storage process for the pre-reduced sample, but this effect will not be discussed in this chapter. Instead, we will focus on the storage of the pre-oxidized catalyst. When the catalyst is exposed to NO<sub>2</sub> only, significant storage is observed (see Fig. 12.8c) and NO is simultaneously produced (Fig. 12.8b) due to the formation of nitrates. The nitrates formed are stable and decompose with a maximum NO<sub>x</sub> desorption of about 400 °C (see Fig. 12.8d). We observed that NO<sub>2</sub> is also adsorbed on the pure zeolite (H-ZSM-5) [11]. In the detailed kinetic model, this feature was modeled separately using a reaction step:



where S2 is an acidic site in the zeolite. The parameters for this storage were later used when modeling the NO<sub>2</sub> storage over Cu-ZSM-5 [11] (see Eq. 12.11). In addition, the following reaction steps were added to describe the NO oxidation:

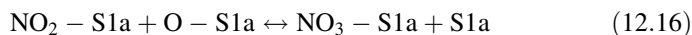




**Fig. 12.8** NO<sub>2</sub> TPD experiment at 200 °C over Cu-CHA. **a** The ratio of NO produced divided by NO<sub>2</sub> consumed. **b** NO concentration in the initial part of the adsorption. **c** NO<sub>2</sub> concentration in the initial part of the adsorption and **d** NO<sub>x</sub> concentration during TPD [36]. Reprinted with permission from Colombo et al. [36]. Copyright (2012) Elsevier

where S1a is the active copper site. In order to simplify the detailed kinetic model [11], an Eley-Rideal mechanism was used for NO oxidation (see Eq. 12.14). Only minor amounts of NO were observed to adsorb on this catalyst, which is why NO storage was not critical to the model. However, it is still possible that the actual mechanism occurs through a Langmuir-Hinshelwood mechanism, but it is not necessary to include this step in the model in order to describe the experimental features.

NO was observed when exposing the catalyst to NO<sub>2</sub>; thus, it is important to add a reaction step whereby nitrites are oxidized by NO<sub>2</sub>, to simultaneously produce nitrates and NO (see Eq. 12.15). Experimentally, we observe that when increasing the temperature and exposing the catalyst to Ar only, nitrates are decomposing. However, the reverse reaction in Eq. (12.15) requires NO in the gas phase and will not take place in pure Ar. Since this is not the case experimentally, an additional step was added in which nitrates decompose directly. In order to make the model thermodynamically consistent, this reaction was also reversible [11].



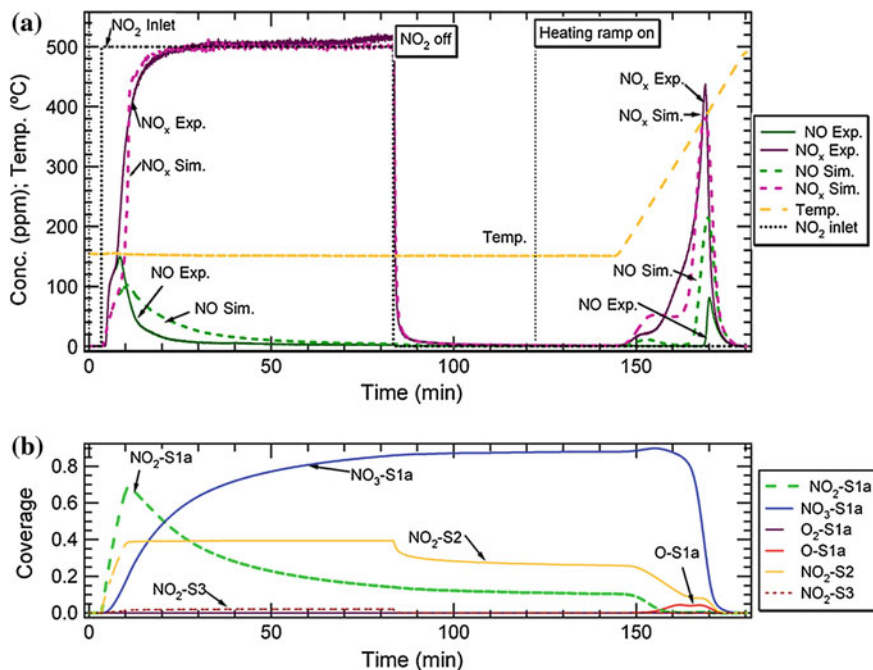


**Fig. 12.9** NO<sub>2</sub> TPD at 150 °C over Cu-ZSM-5 [11]. **a** Solid lines Experiment and dashed lines kinetic model. **b** Calculated mean coverages on the surface. Reprinted with permission from Olsson et al. [11]. Copyright (2009) Elsevier

The results of the experiment (solid line) and the kinetic model (dashed line) for the NO<sub>2</sub> TPD at 150 °C over Cu-ZSM-5 are shown in Fig. 12.9 [11]. The model describes the experimental features adequately. In the lower panel of Fig. 12.9, the coverage on the surface is shown. Based on these results, it becomes evident that nitrites are initially formed on the copper sites and are later converted to nitrates.

An interesting feature was observed involving NO oxidation at low temperature under dry conditions over Cu-ZSM-5. This was observed in an experiment where the catalyst was exposed to NO and oxygen only and the temperature increased in a number of successive steps (30, 50, 100, 30, 50 and 100 °C), see Fig. 12.10 [11]. At 30 °C, substantial NO oxidation to NO<sub>2</sub> is observed. Surprisingly, when increasing the temperature to 50 °C, the NO<sub>2</sub> is decreasing and when further increasing it to 100 °C, the NO oxidation almost vanishes. The behavior is reproducible as seen by increased NO<sub>2</sub> production when the temperature is once again lowered to 30 °C. We suggest that the reason is that at very low temperatures, there are physisorbed species on the surface that account for the low temperature activity. When the temperature increases, the coverage of these species is decreasing, which is also the case with NO oxidation. At higher temperature, the regular NO oxidation takes place, which in the model is occurring on the copper sites. In the detailed kinetic

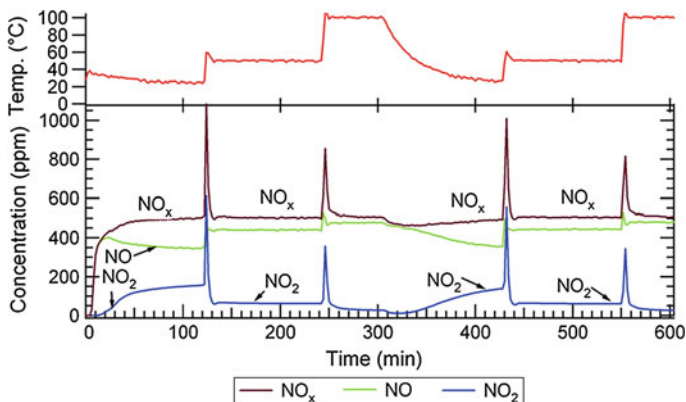
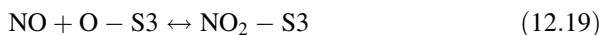


**Fig. 12.10** NO oxidation experiment over Cu-ZSM-5 using 500 ppm NO and 8 % O<sub>2</sub> and changing the temperature stepwise (30, 50, 100, 30, 50 and 100 °C) [11]. Reprinted with permission from Olsson et al. [11]. Copyright (2009) Elsevier

model, three reversible reactions were added in order to describe the low temperature NO oxidation:



where S3 denotes a site for physisorbed species.

The combination of reactions (12.10–12.19) was used in the kinetic model for NO<sub>x</sub> storage and NO oxidation under dry conditions over a large temperature interval, with the results shown in Fig. 12.11. The model accurately describes the NO oxidation, both at low and high temperature [11]. At high temperatures, the NO oxidation activity drops because of thermodynamic restrictions. The lower panel in Fig. 12.11 shows the mean coverages on the surface; it becomes clear that the S3 site is only active at low temperature because at higher temperatures, the coverage on this site is very low. In addition, due to the decomposition of nitrates, NO<sub>x</sub> is desorbing from the surface when the temperature between steps increases.

NO oxidation in the presence of water is simulated using a detailed kinetic model [12], where NO oxidation on Cu-ZSM-5 [11], the above described water adsorption [13] and OH formation [12] are used together (Fig. 12.12). The model describes the significantly lower NO oxidation observed in the experiment due to the blocking of OH groups on the active copper site (S1a) seen in the coverages in the lower panel of Fig. 12.12 [12]. In addition, water blocks the NO<sub>2</sub> storage and, therefore, only very small amounts of NO<sub>x</sub> are desorbing when the temperature between steps increases. It should be mentioned that during NO oxidation, both NO and NO<sub>2</sub> are simultaneously present. The NO will destabilize the nitrates and thereby, less NO<sub>x</sub> is stored.

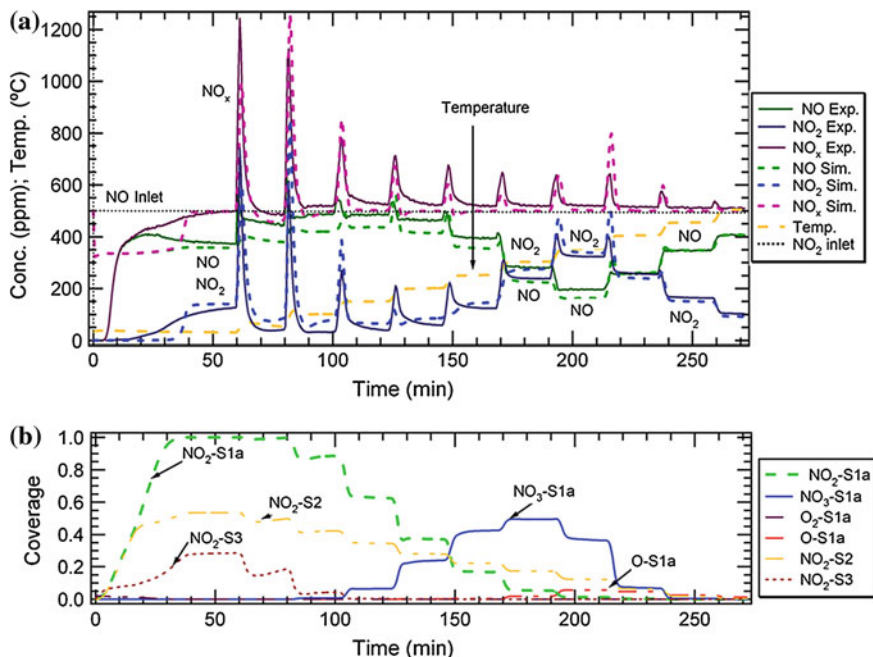


**Fig. 12.11** NO oxidation experiment (500 ppm NO and 8 % O<sub>2</sub>) and increasing the temperature stepwise over Cu-ZSM-5 [11]. **a** Solid lines Experiment and dashed lines kinetic model. **b** Calculated mean coverages on the surface. Reprinted with permission from Olsson et al. [11]. Copyright (2009) Elsevier

### 12.4.2 Global Kinetic Model for NO Oxidation

Metkar et al. [9] developed a global kinetic model from a derivation of detailed reaction steps. They used reactions described in (12.11–12.14 [11]) and combined two reactions (see Eqs. 12.15–12.16 [11]). They received the best results when assuming the Eley-Rideal step, during the NO oxidation (Eq. 12.14) as rate determining. The resulting rate expression was:

$$R_{NO_{oxi}} = \frac{k_{f3}\sqrt{k_1k_2}}{1 + K_1X_{O_2,s} + \sqrt{K_1K_2X_{O_2,s}} + K_4X_{NO_2,s} + \sqrt{\frac{K_5'K_4^3X_{NO_2,s}^3\sqrt{K_1K_2X_{O_2,s}}}{X_{NO,S}}}} \left( X_{NO,S}\sqrt{X_{O_2,s}} - \frac{X_{NO_2,S}}{K_{eq}} \right) \quad (12.20)$$

The results from this global NO oxidation model is shown in Fig. 12.13 [9]. In this figure, results from both Fe-ZSM-5 (solid lines) and Cu-CHA are shown (dashed lines). The markers show the experimental points. The model accurately

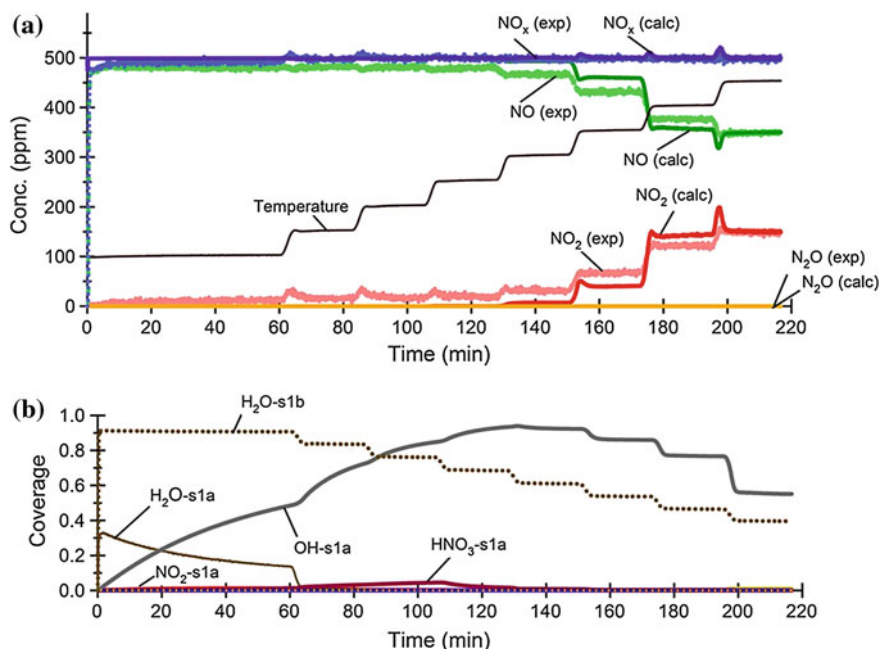
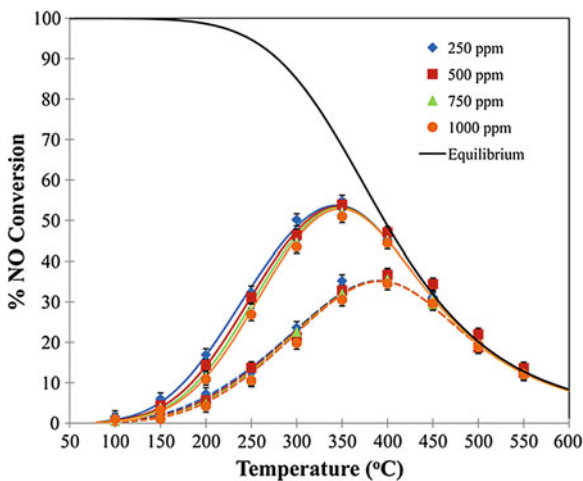


**Fig. 12.12** NO oxidation experiment in the presence of water (500 ppm NO, 8 % O<sub>2</sub> and 5 % H<sub>2</sub>O) and increasing the temperature stepwise over Cu-ZSM-5 [12]. **a** Solid lines Experiment and dashed lines kinetic model. **b** Calculated mean coverages on the surface. Reprinted with permission from Sjövall et al. [12]. Copyright (2009) Elsevier

**Fig. 12.13** NO oxidation in dry conditions (250–1000 ppm NO and 5 % O<sub>2</sub>) over Fe-ZSM-5 (solid lines) and Cu-CHA (dashed lines). Symbols Experimental data, continuous lines model [9]. Reprinted with permission from Metkar et al. [9]. Copyright (2012) Elsevier

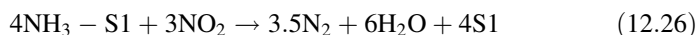
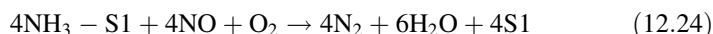
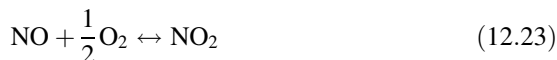
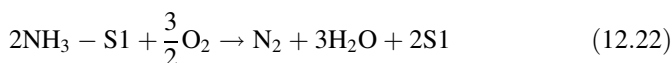


describes the experimental observations for various NO concentrations over the whole temperature interval. In the work by Olsson et al. [10] a kinetic model for NO oxidation is also included.

## 12.5 Kinetic Models for SCR Reactions Over Cu-Zeolites

### 12.5.1 Global Kinetic Models for SCR Over Cu-Zeolites

We developed a global kinetic model for ammonia SCR over Cu-ZSM-5 [10], consisting of seven reaction steps:



The first step is ammonia adsorption/desorption and this step was tuned to an ammonia TPD experiment described in an earlier section (Eq. 12.21, see Fig. 12.4). The second step is ammonia oxidation (Eq. 12.22) and the third step NO oxidation (Eq. 12.23). The parameters for these three steps were determined by separate experiments. In Eq. (12.24), the reaction for standard SCR is described and in Eq. (12.25), the rapid SCR with equimolar amounts of NO and NO<sub>2</sub> is covered. NH<sub>3</sub> also reacts with NO<sub>2</sub> alone, which is described in Eq. (12.26). The final step (see Eq. 12.27) is N<sub>2</sub>O production from a reaction between adsorbed ammonia and NO<sub>2</sub>. The results from exposing the Cu-ZSM-5 catalyst to 500 ppm NO, 500 ppm NH<sub>3</sub>, 8 % O<sub>2</sub> and 5 % H<sub>2</sub>O, while increasing the temperature stepwise are shown in Fig. 12.14 [10]. Initially, there is a total uptake of ammonia for an extended time period, but due to minor NO storage, NO breaks through immediately. The temperature is then increased to about 150 °C, while loosely bound ammonia is released. At this temperature, the standard SCR reaction is active and equimolar consumption of NO and NH<sub>3</sub> is seen. At 200 °C, the conversion of NO<sub>x</sub> is close to 100 %. At high temperature, the NO<sub>x</sub> conversion again decreases due to the ammonia oxidation. Also, some NO<sub>2</sub> is produced, since the back part of the catalyst is not exposed to ammonia, NO oxidation may occur. The global model described

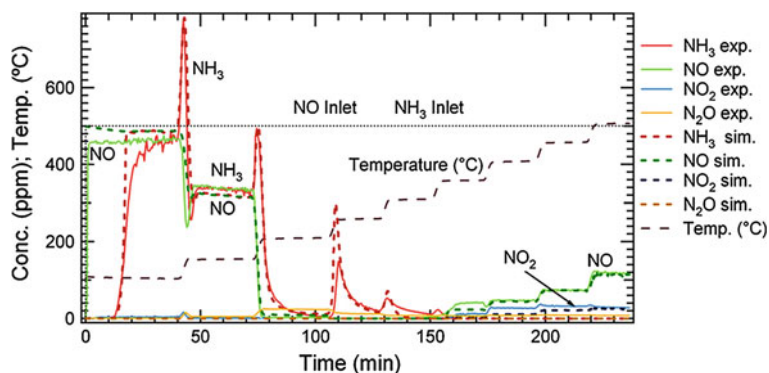


**Fig. 12.14** NO, NO<sub>2</sub>, NH<sub>3</sub> and N<sub>2</sub>O concentration from experiment (solid line) and model (dashed line) after exposing the Cu-ZSM-5 catalyst to 500 ppm NO, 500 ppm NH<sub>3</sub>, 8 % O<sub>2</sub> and 5 % H<sub>2</sub>O and stepwise increasing the temperature [10]. Reprinted with permission from Olsson et al. [10]. Copyright (2008) Elsevier

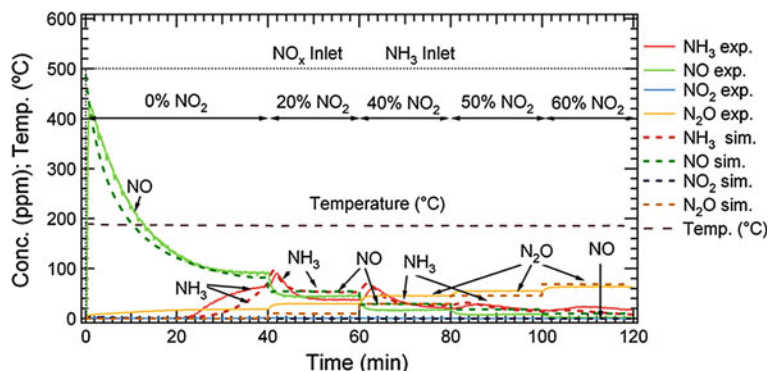


**Fig. 12.15** NO, NO<sub>2</sub>, NH<sub>3</sub> and N<sub>2</sub>O concentration from experiment (solid line) and model (dashed line) after exposing the Cu-ZSM-5 catalyst to 500 ppm NO<sub>x</sub>, 500 ppm NH<sub>3</sub>, 8 % O<sub>2</sub> and 5 % H<sub>2</sub>O and stepwise increasing the NO<sub>2</sub> content [10]. Reprinted with permission from Olsson et al. [10]. Copyright (2008) Elsevier

was developed based on a series of experiments with a variety of gas compositions and over a broad temperature range [10]. In Fig. 12.15, results from an experiment and corresponding model are illustrated while changing the NO<sub>2</sub> to NO<sub>x</sub> ratio from 0 % up to 60 %, with an inlet gas temperature of 175 °C. Prior to this experiment, the catalyst was pretreated with oxygen at high temperature in order to clean the surface from ammonia. The Cu-ZSM-5 catalyst is exposed to the gas mixture (500 ppm NO, 500 ppm NH<sub>3</sub>, 500 ppm O<sub>2</sub>, and 5 % H<sub>2</sub>O) from the inception of the experiment. During the first 20 min, no ammonia is detected because the storage of substantial amounts of ammonia on the surface, in combination with that ammonia is consumed in the SCR reaction. The NO concentration is decreasing from over

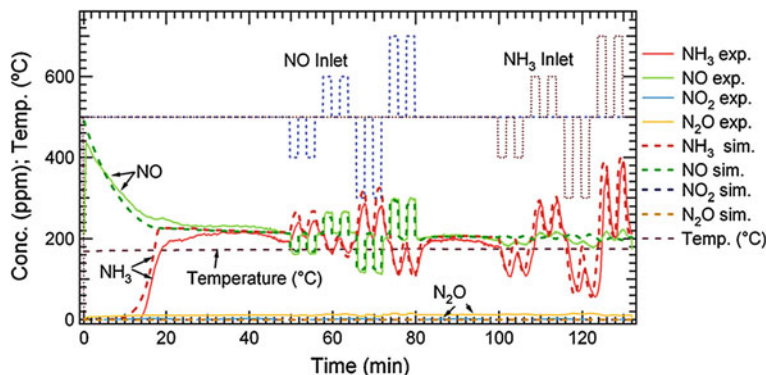


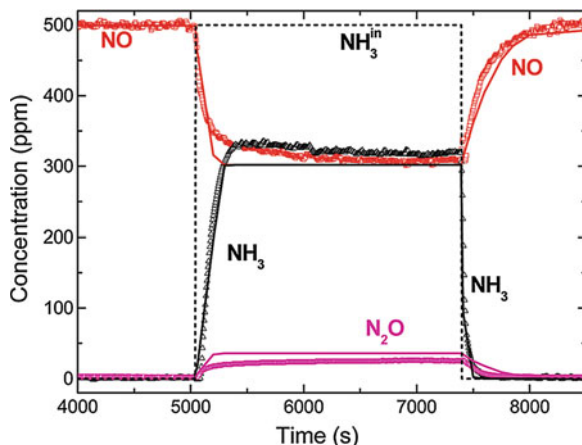
**Fig. 12.16** NO, NO<sub>2</sub>, NH<sub>3</sub>, and N<sub>2</sub>O concentration from a validation experiment (*solid line*) and model (*dashed line*) after exposing the Cu-ZSM-5 catalyst to 500 ppm NO<sub>x</sub>, 500 ppm NH<sub>3</sub>, 8 % O<sub>2</sub>, and 5 % H<sub>2</sub>O and thereafter changing NO and NH<sub>3</sub> concentrations in short steps [10]. Reprinted with permission from Olsson et al. [10]. Copyright (2008) Elsevier

400 ppm down to approx. 100 ppm. The reason for this decrease, which is also accurately described in the model, is that the SCR rate depends on the coverage of ammonia on the surface. The ammonia coverage is increasing over time, which results in an increased SCR reaction rate and, thereby, higher NO conversion. Further, when increasing the NO<sub>2</sub> content, the activity for NO<sub>x</sub> reduction increases and reaches a maximum at 50–60 % of the NO<sub>2</sub> to NO<sub>x</sub> ratio. At higher NO<sub>2</sub> levels, the activity over Cu-zeolites [8] again decreases. In addition, the N<sub>2</sub>O concentration is increasing with increasing NO<sub>2</sub> fraction, which is explained by the last reaction (Eq. 12.27).

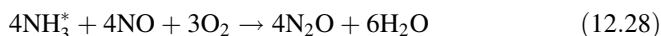
In kinetic model development, it is crucial to validate the model with experiments not included during the development of the model. The results in Fig. 12.16 illustrate a validation experiment [10]. In this experiment, the catalyst is initially exposed to 500 ppm NO, 500 ppm NH<sub>3</sub>, 8 % O<sub>2</sub>, and 5 % H<sub>2</sub>O and when a steady state is reached, the concentration of NO and thereafter ammonia is altered in short steps. Interestingly, when the NO concentration changes, the NO outlet also rapidly changes, but when performing the corresponding change in ammonia concentration, the NO level remains practically constant due to the large buffering of ammonia on the surface. The ammonia coverage is similar during the 2 min time, when the ammonia level is changed because the ammonia storage on the catalyst is excessive. Since the SCR rate depends on the coverage of ammonia on the surface as opposed to the gas phase, this results in the same SCR rate, which is why the NO conversion is practically the same.

Nova et al. [37] presented a global kinetic model for ammonia SCR over a Cu-zeolite catalyst. They used the same seven reactions as presented above (Eqs. 12.21–12.27). In addition, they added two more reactions. In the first reaction (Eq. 12.28), N<sub>2</sub>O is formed from a reaction between ammonia on the surface (denoted NH<sub>3</sub><sup>\*</sup>) and NO and in the second reaction, ammonium nitrate is formed

**Fig. 12.17** Transient SCR experiment at 200 °C over Cu zeolite. In this experiment, the catalyst is exposed to (1) 500 ppm NO, 8 % O<sub>2</sub>, 5 % H<sub>2</sub>O (2) 500 ppm NO, 500 ppm NH<sub>3</sub>, 8 % O<sub>2</sub>, 5 % H<sub>2</sub>O, and (3) 500 ppm NO, 8 % O<sub>2</sub>, 5 % H<sub>2</sub>O [37]. Reprinted with permission from Nova et al. [37]. Copyright (2011) American Chemical Society

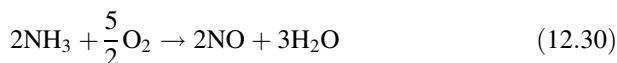


during a reaction with ammonia on the surface and NO<sub>2</sub> in the gas phase (Eq. 12.29).



The results from this model are shown in Fig. 12.17, where a transient experiment is conducted at 200 °C. The ammonia concentration drops fast, while the NO concentration slowly increases, when turning off ammonia during step three. The reason is that there are large amounts of ammonia adsorbed on the surface, which is why the SCR reaction can continue for a substantial amount of time until the ammonia coverage is zero. The model can describe the experimental findings well [37]. The model presented by Nova et al. [37] was also used to simulate experiments during which the NO<sub>2</sub> to NO<sub>x</sub> ratio varied. The results from these experiments and the corresponding model are shown in Fig. 12.18 [37], where Fig. 12.18a shows the NO<sub>x</sub> conversion, Fig. 12.18b the NH<sub>3</sub> conversion, and Fig. 12.18c the N<sub>2</sub>O formation. The NO<sub>x</sub> conversion is at a maximum for the NO<sub>2</sub> to NO<sub>x</sub> ratio of 66 % and decreases when the NO<sub>2</sub> level further increases because the slower NO<sub>2</sub> SCR reaction dominates. The N<sub>2</sub>O production shows a maximum at lower temperatures, likely due to that ammonium nitrate is an intermediate for N<sub>2</sub>O production and ammonium nitrates decompose at high temperatures.

Pant and Schmiege [7] used the model developed by Olsson et al. [10] (see Eqs. 12.21–12.27) with one exception. Instead of ammonia oxidation to N<sub>2</sub>, as described in Eq. (12.22), ammonia oxidation to NO was used:



One of the reasons was that they observed NO formation over their catalyst at high temperatures. Pant and Schmiege [7] investigated the influence of changing the

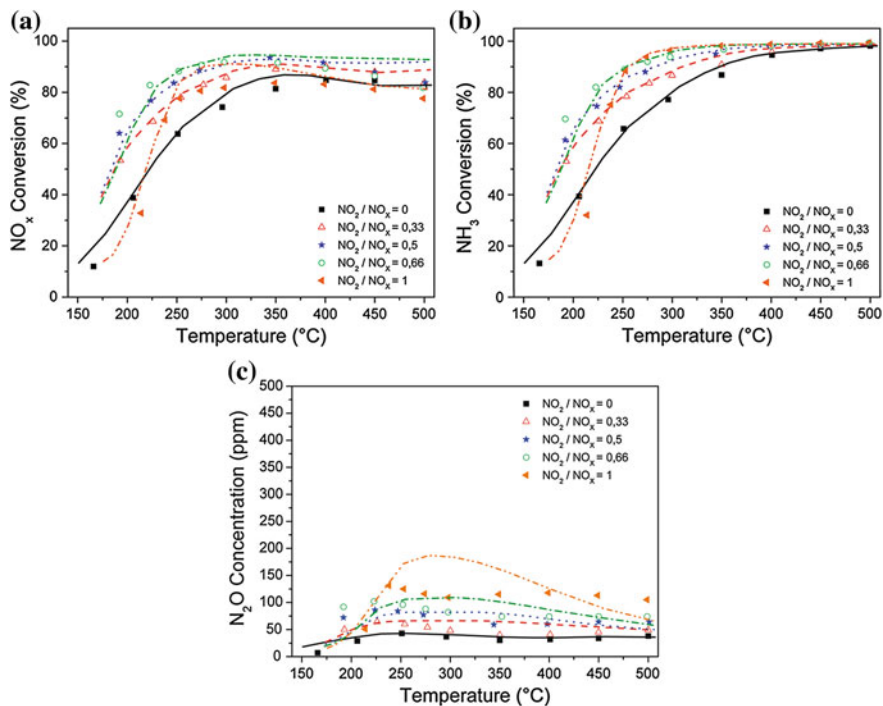


**Fig. 12.18** Experiment (markers) and kinetic model (solid lines), when exposing a Cu-zeolite to 500 ppm NO<sub>x</sub>, 500 ppm NH<sub>3</sub>, 8 % O<sub>2</sub> and 5 % H<sub>2</sub>O and varying the NO<sub>2</sub> content [37]. Reprinted with permission from Nova et al. [37]. Copyright (2011) American Chemical Society

space velocity (the gas composition was also varied), with the results presented in Fig. 12.19. In these experiments, real diesel exhaust and urea injection have been used.

Baik et al. [38] simulated urea SCR and included the following equations for the concentration of urea, HNCO, NO, and NH<sub>3</sub>:

$$\frac{dC_{\text{Urea}}}{d\tau} = -k_3 C_{\text{Urea}} \quad (12.31)$$

$$\frac{dC_{\text{HNCO}}}{d\tau} = k_3 C_{\text{Urea}} - k_4 C_{\text{HNCO}} C_{\text{H}_2\text{O}} \quad (12.32)$$

$$-\frac{dC_{\text{NO}}}{d\tau} = \frac{K_1 C_{\text{NO}} C_{\text{NH}_3}}{(1 + K_{\text{NO}} C_{\text{NO}})(1 + K_{\text{NH}_3} C_{\text{NH}_3})} \quad (12.33)$$

$$-\frac{dC_{\text{NH}_3}}{d\tau} = \frac{K_1 C_{\text{NO}} C_{\text{NH}_3}}{(1 + K_{\text{NO}} C_{\text{NO}})(1 + K_{\text{NH}_3} C_{\text{NH}_3})} + \frac{k_2 C_{\text{NH}_3}}{(1 + K_{\text{NH}_3} C_{\text{NH}_3})} \quad (12.34)$$

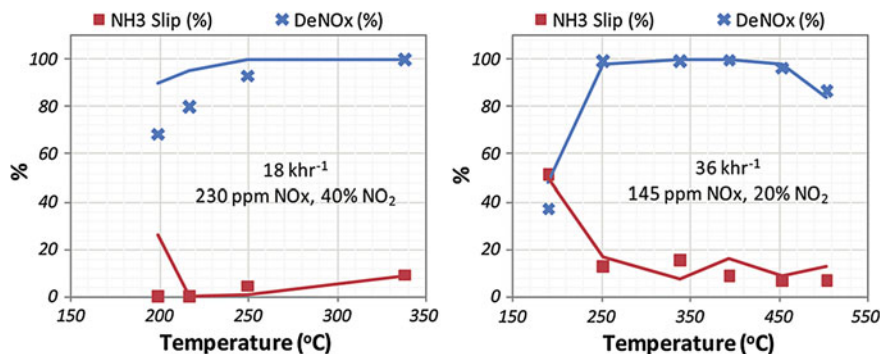
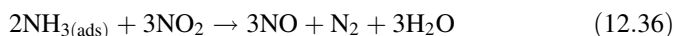
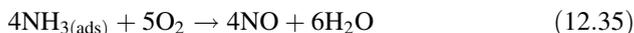


**Fig. 12.19** Ammonia slip and deNO<sub>x</sub> activity versus exhaust temperature for a Cu-zeolite. The NH<sub>3</sub>/NO<sub>x</sub> ratio was 1.3. The NO<sub>x</sub> concentration and space velocity is shown in the panels [7]. The symbols represent the experimental points and the solid lines the model. Reprinted with permission from Pant and Schmiege [7]. Copyright (2011) American Chemical Society

The results from this model, when varying the space velocity, are shown in Fig. 12.20 [38]. In these experiments, urea was used as an ammonia source and the thermal decomposition of urea was conducted at 350 °C in order to completely decompose urea into ammonia and HNCO [39].

Watling et al. [40] used a kinetic model for simulating the New European Drive Cycle (NEDC) test over a Cu-zeolite coated filter. The reactions used to describe the SCR system are shown in Eqs. (12.21–12.27) in addition to the following two reactions:



In the first reaction (Eq. 12.35), ammonia is oxidized to NO, a step that was also used by Pant and Schmiege [7]. In the second reaction, NO<sub>2</sub> is reduced to NO by reacting with ammonia. The model is used to describe the cumulative NO<sub>x</sub> during an NEDC test and the results from the test and model are shown in Fig. 12.21. The model accurately describes the cumulative NO<sub>x</sub>.

### 12.5.2 Detailed Kinetic Models for SCR Over Cu-Zeolites

A detailed kinetic model was developed [11–13] and constructed out of several submodels previously described in this chapter. The different sites used in the model is discussed in Sect. 12.2.2. The submodels include: (i) ammonia adsorption/desorption, (ii) water adsorption/desorption, (iii) ammonia oxidation, (iv) NO<sub>2</sub> storage, and (v) NO oxidation. The results of these studies were used in developing

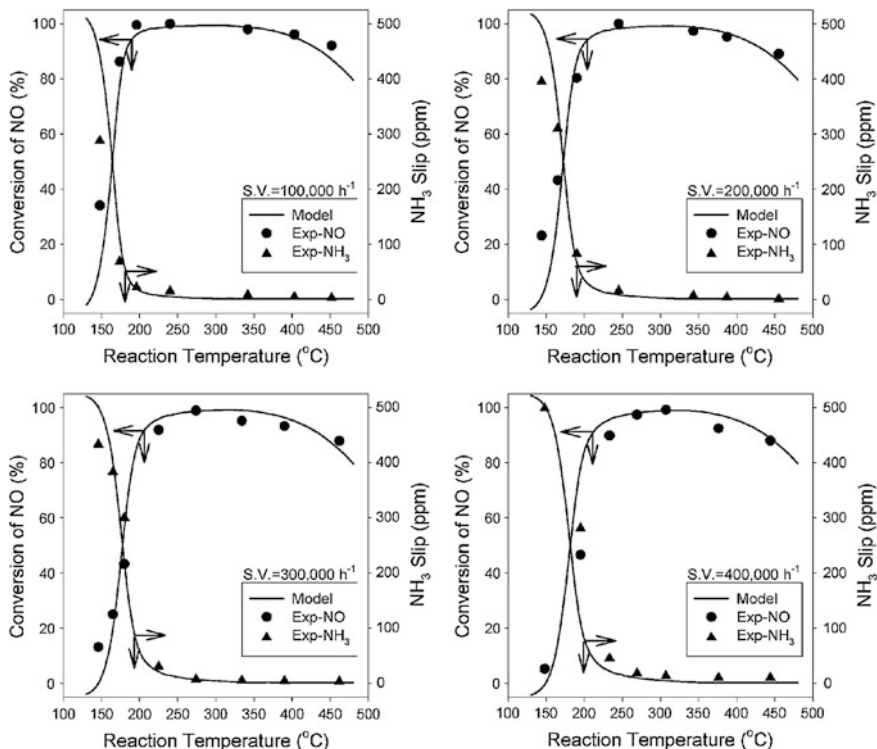
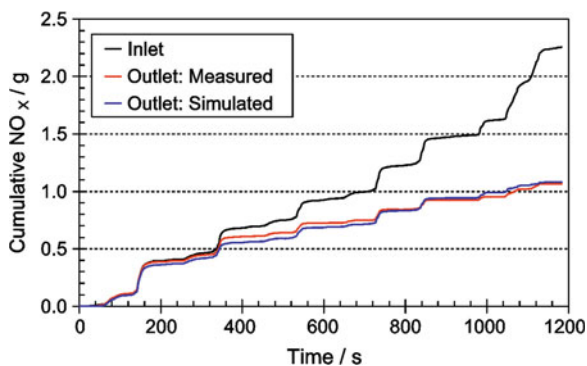
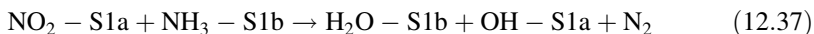


**Fig. 12.20** Urea SCR over Cu-ZSM-5, when varying space velocity [38]. Reprinted with permission from Baik et al. [38]. Copyright (2006) American Chemical Society

**Fig. 12.21** Measured and simulated cumulative NO<sub>x</sub> using a Cu-zeolite coated DPF (denoted Cu-SCR<sup>®</sup>) in an NEDC test [40]. Reprinted with permission from Watling et al. [40]. Copyright (2012) Elsevier



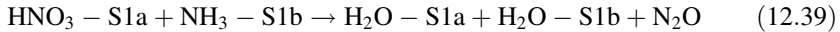
the SCR steps. In the first SCR reaction, formed nitrites react with adsorbed ammonia according to:



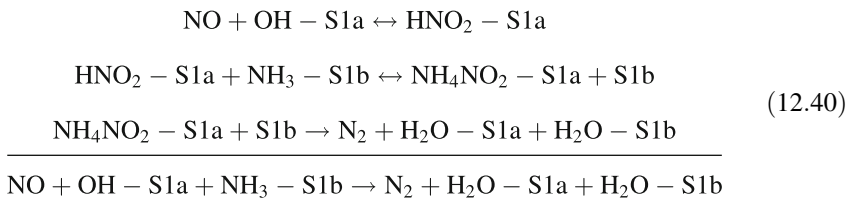
In the presence of water, it is likely that  $\text{HNO}_3$  is formed on the surface, which have been suggested for SCR over vanadia catalysts [41]. We have, therefore, added a reaction step to form  $\text{HNO}_3$  (Eq. 12.38).



$\text{HNO}_3$  can then react with ammonia on the surface to produce ammonium nitrate, which can decompose to produce  $\text{N}_2\text{O}$ . In order to simplify the model, these two steps in the model are described as one step:

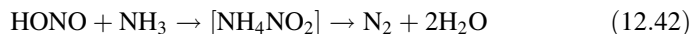


Further, it is suggested that  $\text{HNO}_2$  is formed over vanadia, and then produces ammonium nitrite, which rapidly decomposes to produce water and  $\text{N}_2$  [41]. This mechanism was also used to derive the last step in the detailed model (Eq. 12.40) [12]:



The model was developed through a large set of experiments, during which gas composition and temperature varied [12], and below are two illustrated examples. In the first experiment, the Cu-ZSM-5 catalyst was exposed to 500 ppm NO, 8 %  $\text{O}_2$ , and the ammonia concentration varied from 200 to 800 ppm in steps to 175 °C. The results of the experiment and model are shown in Fig. 12.22, in which the top panel shows the concentrations and the lower panel shows the calculated mean coverage on the surface. The results of the coverages from the model show that on the S1a (active copper site), the dominant species at lower ammonia concentrations is nitrites ( $\text{NO}_2\text{-S1a}$ ), but some nitrates are also present. At higher ammonia concentrations, the nitrite coverage decreases simultaneously as the ammonia coverage increases. This experiment was repeated with 5 % water present and a 50 %  $\text{NO}_2$  to  $\text{NO}_x$  ratio. The results are shown in Fig. 12.23. The  $\text{NO}_2$  content, in combination with high water levels, results in larger  $\text{HNO}_3$  coverage on the active copper sites (see reaction in Eq. 12.38), which gives a higher rate of  $\text{N}_2\text{O}$  production (see Eq. 12.39), and is visible by the higher  $\text{N}_2\text{O}$  concentration in the experiment, as well as in the model.

Grossale et al. [8] present a detailed kinetic model for ammonia SCR over Fe and Cu-zeolites, where the  $\text{NO}_2$  reactions are described by the following steps:



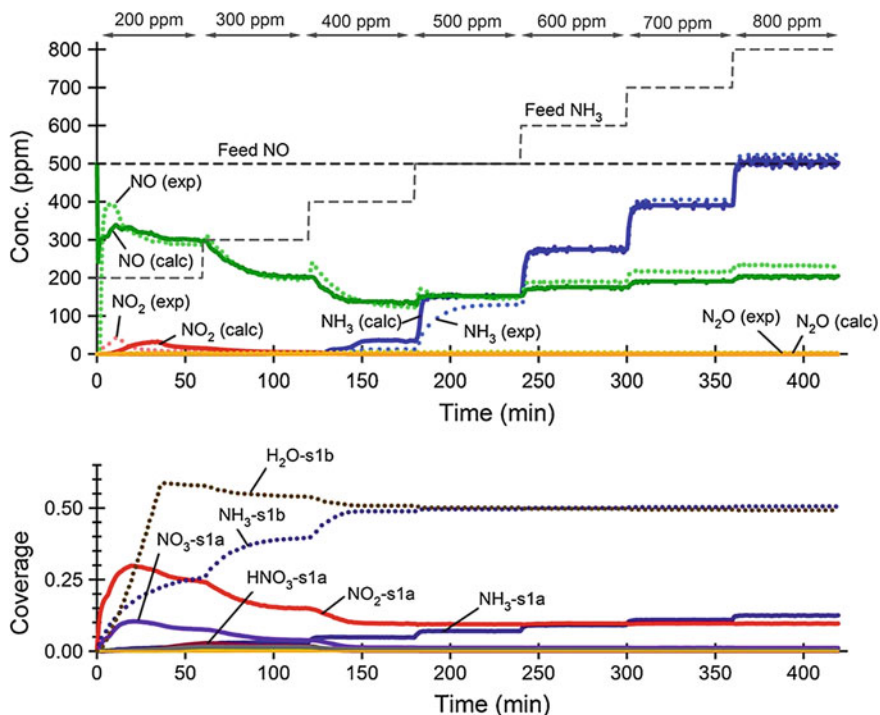
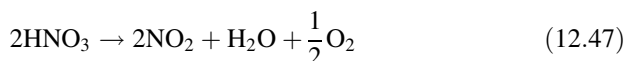
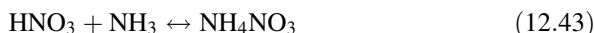


**Fig. 12.22** Experiment (*dotted lines*) and model (*solid lines*), from a test where a Cu-ZSM-5 catalyst was exposed to 500 ppm NO, 8 % O<sub>2</sub>, and varying the ammonia concentration from 200 to 800 ppm in steps at 175 °C. The lower panel shows the mean calculated coverages on the surface [12]. Reprinted with permission from Sjövall et al. [12]. Copyright (2009) Elsevier



These reactions are used together with reactions, e.g., for standard SCR, ammonia spillover [8] and the results from the model to describe NO<sub>2</sub>/NO<sub>x</sub> variations for Cu-zeolite, as shown in Fig. 12.24. The model accurately describes the NO<sub>2</sub>/NO<sub>x</sub> dependence across a broad temperature interval.

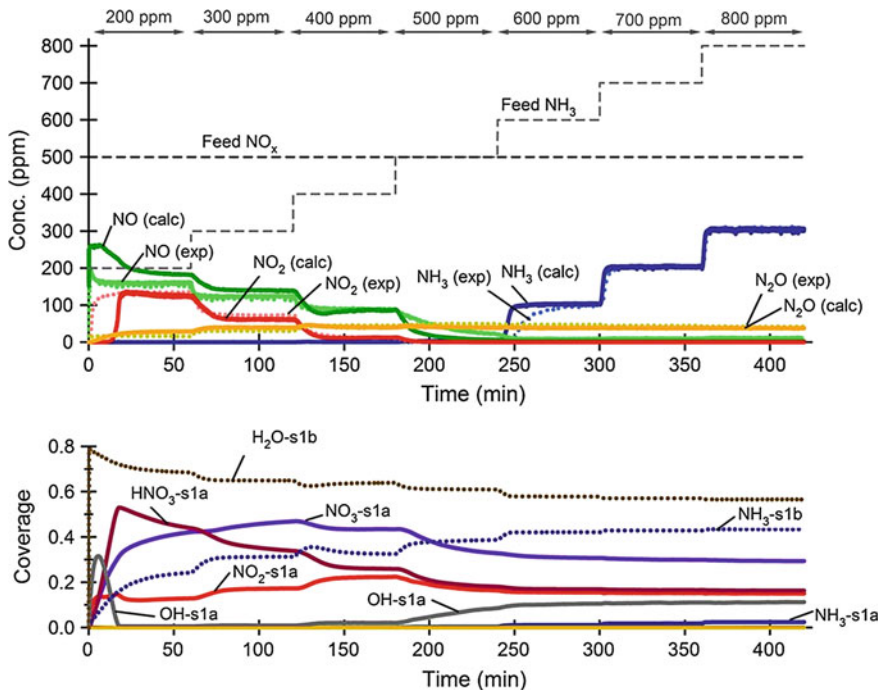
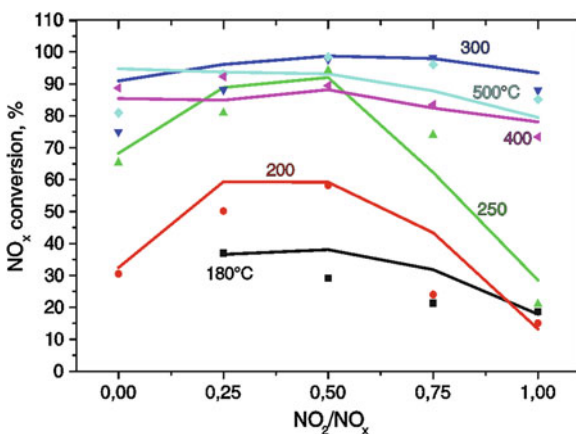


**Fig. 12.23** Experiment (dotted lines) and model (solid lines), from a test where a Cu-ZSM-5 catalyst was exposed to 250 ppm NO, 250 ppm NO<sub>2</sub>, 8 % O<sub>2</sub>, 5 % H<sub>2</sub>O and varying the ammonia concentration from 200 to 800 ppm in steps at 175 °C. The lower panel shows the calculated mean coverages on the surface [12]. Reprinted with permission from Sjövall et al. [12]. Copyright (2009) Elsevier

**Fig. 12.24** SCR experiments when varying NO<sub>2</sub> to NO<sub>x</sub> ratio over a Cu-zeolite at different temperatures. The inlet feed gas consists of 500 ppm NO<sub>x</sub>, 500 ppm NH<sub>3</sub>, 3 % H<sub>2</sub>O and 2 % O<sub>2</sub>. Solid lines (kinetic model) and symbols (experiment) [8]. Reprinted with permission from Grossale et al. [8]. Copyright (2009) Springer



## 12.6 Conclusions

This chapter is a review of the state of the art in kinetic modeling of ammonia/urea SCR over copper containing zeolites. Both fundamental detailed kinetic models as well as more globalized models are discussed. Several submodels are studied for the SCR system: (i) ammonia adsorption and desorption, (ii) NO<sub>2</sub> adsorption and desorption, (iii) water adsorption and desorption, (iv) ammonia oxidation, (v) NO oxidation, (vi) standard SCR, (vii) rapid SCR, (viii) slow NO<sub>2</sub> SCR, (ix) N<sub>2</sub>O formation, and (x) urea decomposition and hydrolysis to produce ammonia. As can be seen from this large number of steps, this is a complex system.

A good description of the ammonia storage and desorption is critical in order to describe transient features of the SCR system, and usually a Temkin type of kinetics is used that considers the adsorbate–adsorbate interactions. The parameters for these reactions are usually fitted to TPD experiments, but also microcalorimetry studies are presented. The most common approach is to consider one ammonia adsorption site, but more detailed kinetic models use several adsorption sites. Ammonia oxidation is a reaction occurring at high temperatures, which unfortunately decreases the selectivity of the NO<sub>x</sub> reduction in SCR. It is therefore crucial to include this reaction in kinetic models for this system.

Different SCR reaction occurs depending on the NO<sub>2</sub> to NO<sub>x</sub> ratio, where standard SCR occurs with NO only, rapid SCR with equimolar amount of NO and NO<sub>2</sub>, and slow NO<sub>2</sub> SCR with NO<sub>2</sub> only. In several global kinetic models, these three reactions are added. In more detailed models, more surface species are considered, for example, nitrites, nitrates, HNO<sub>3</sub>, oxygen, and hydroxyls. N<sub>2</sub>O is an unwanted by-product during the SCR process over copper zeolites that are increasing with the NO<sub>2</sub> content. The mechanism for the N<sub>2</sub>O production is suggested to be from decomposition of ammonium nitrate. In addition, there are models available that incorporate the urea decomposition and hydrolysis, in addition to the SCR reactions.

## References

1. H. Sjövall, L. Olsson, E. Fridell, and R. J. Blint, *Applied Catalysis B* 64 (2006) 180.
2. H. Sjövall, E. Fridell, R. J. Blint, and L. Olsson, *Topics in Catalysis* 42–43 (2007) 113.
3. J.-H. Park, H. J. Park, J. H. Baik, I.-S. Nam, C.-H. Shin, J.-H. Lee, B. K. Cho, and S. H. Oh, *Journal of Catalysis* 240 (2006) 47.
4. S. Kieger, G. Delahay, B. Coq, and B. Neveu, *Journal of Catalysis* 183 (1999) 267.
5. J. A. Sullivan, J. Cunningham, M. A. Morris, and K. Keneavey, *Applied Catalysis B: Environmental* 7 (1995) 137.
6. K. Rahkamaa-Tolonen, T. Maunula, M. Lomma, M. Huuhtanen, and R. L. Keiski, *Catalysis Today* 100 (2005) 217.
7. A. Pant and S. J. Schmiege, *Industrial & Engineering Chemistry Research* 50 (2011) 5490.
8. A. Grossale, I. Nova, E. Tronconi, D. Chatterjee, and M. Weibel, *Topics in Catalysis* 52 (2009) 1837.

9. P. S. Metkar, V. Balakotaiah, and M. P. Harold, *Catalysis Today* 184 (2012) 115.
10. L. Olsson, H. Sjövall, and R. J. Blint, *Applied Catalysis B-Environmental* 81 (2008) 203.
11. L. Olsson, H. Sjövall, and R. J. Blint, *Appl. Catal. B: Environmental*. 87 (2009) 200.
12. H. Sjövall, R. J. Blint, and L. Olsson, *Appl. Catal. B* 92 (2009) 138.
13. H. Sjövall, L. Olsson, and R. J. Blint, *J. Phys Chem. C* 113 (2009) 1393.
14. G. Delahay, S. Kieger, N. Tanchoux, P. Trens, and B. Coq, *Applied Catalysis B: Environmental* 52 (2004) 251.
15. N. Wilken, K. Wijayanti, K. Kamasamudram, N. W. Currier, R. Vedaiyan, A. Yezerets, and L. Olsson, *Appl. Catal. B* 111 (2012) 58.
16. N. Wilken, K. Kamasamudram, N. W. Currier, J. Li, A. Yezerets, and L. Olsson, *Catalysis Today* 151 (2010) 237.
17. A. Delabie, K. Pierloot, M. H. Groothaert, B. M. Weckhuysen, and A. Schoonheydt, *Microporous and mesoporous materials* 27 (2000) 209.
18. J. H. Kwak, D. Tran, S. D. Burton, J. Szanyi, J. H. Lee, and C. H. F. Peden, *Journal of Catalysis* 289 (2012) 272.
19. L. Wang, W. Li, G. S. Qi, and D. Weng, *Journal of Catalysis* 289 (2012) 21.
20. I. Nova, L. Lietti, E. Tronconi, and P. Forzatti, *Chemical Engineering Science* 56 (2001) 1229.
21. B. Roduit, A. Wokaun, and A. Baiker, *Industrial & Engineering Chemistry Research* 37 (1998) 4577.
22. J. A. Dumesic, N.-Y. Topsoe, H. Topsoe, Y. Chen, and T. Slabiak, *Journal of Catalysis* 163 (1996) 409.
23. L. Lietti, I. Nova, E. Tronconi, and P. Forzatti, *Catal. Today* 45 (1998).
24. D. Chatterjee, T. Burkhardt, M. Weibel, E. Tronconi, I. Nova, and C. Ciardelli, *SAE 2006-01-0468* (2006).
25. S. A. Stevenson, J. C. Vartuli, and C. F. Brooks, *Journal of Catalysis* 190 (2000) 228.
26. S. Malmberg, M. Votsmeier, J. Gieshoff, N. Söger, L. Mußmann, A. Schuler, and A. Drochner, *Topics in Catalysis* 42–43 (2007) 33.
27. D. Chatterjee, T. Burkhardt, M. Weibel, I. Nova, A. Grossale, and E. Tronconi, *SAE 2007-01-1136* (2007).
28. H. Sjövall, R. J. Blint, A. Gopinath, and L. Olsson, *Industrial & Engineering Chemistry Research* 49 (2010) 39.
29. E. Tronconi, I. Nova, C. Ciardelli, D. Chatterjee, B. Bandl-Konrad, and T. Burkhardt, *Catalysis Today* 105 (2005) 529.
30. C. Busco, A. Barbaglia, M. Broyer, V. Bolis, G. M. Foddanu, and P. Ugliengo, in *Thermochimica Acta* Vol. 418 (1–2), 2004, p. 3.
31. P. Felix, C. Savill-Jowitt, and D. R. Brown, *Thermochimica Acta* 433 (2005) 59.
32. G. Boskovic, T. Vulic, E. Kis, and P. Putanov, *Chemical Engineering & Technology* 24 (2001) 269.
33. W. B. Williamson, D. R. Flentge, and J. H. Lunsford, *J. of Catal.* 37 (1975) 258.
34. W. B. Williamson and J. H. Lunsford, *J. of Phys. Chem.* 80 (1976) 2664.
35. T. Komatsu, M. Nunokawa, I. S. Moon, T. Takahara, S. Namba, and T. Yashima, *Journal of Catalysis* 148 (1994) 427.
36. M. Colombo, I. Nova, and E. Tronconi, *Applied Catalysis B-Environmental* 111 (2012) 433.
37. I. Nova, D. Bounechada, R. Maestri, E. Tronconi, A. K. Heibel, T. A. Collins, and T. Boger, *Industrial & Engineering Chemistry Research* 50 (2011) 299.
38. J. H. Baik, S. D. Yim, I. S. Nam, Y. S. Mok, J. H. Lee, B. K. Cho, and S. H. Oh, *Industrial & Engineering Chemistry Research* 45 (2006) 5258.
39. S. D. Yim, S. J. Kim, J. H. Baik, I.-S. Nam, Y. S. Mok, J.-H. Lee, B. K. Cho, and S. H. Oh, *Ind. Eng. Chem. Res.* 43 (2004) 4856.
40. T. C. Watling, M. R. Ravenscroft, and G. Avery, *Catalysis Today* 188 (2012) 32.
41. C. Ciardelli, I. Nova, E. Tronconi, D. Chatterjee, T. Burkhardt, and M. Weibel, *Chemical Engineering Science* 62 (2007) 5001.